LA-UR- 11-05017

Approved for public release;
distribution is unlimited.

Title:	Modeling Turbulent Mixing
Author(s):	Baolian Cheng
Intended for:	Proceedings of 17th Biennial International Conference of the APS Topic Group on Shock Compression of Condensed Matter(AIP Journal)

Form 836 (7/06)

MODELING TURBULENT MIXING

Baolian Cheng

Los Alamos National Laboratory, NM 87545

Abstract. Fluid mixing is an important phenomenon in many physical applications from supernova explosions to genetic structure formations. Moving interfaces between distinct fluids in a multi-fluid system are often unstable. Small perturbations at such interfaces grow as a result of nonlinear hydrodynamic processes, and evolve into turbulent mixing regions. In this work, we present theoretical models to predict the mixing growth rates and numerical simulations for the chaotic mixing fluids. Our results are in good agreement with experiments.

Keywords: Hydrodynamic instabilities, turbulent mix
PACS: 47.20.Ma, 47.52.+j

INTRODUCTION

Three major types of hydrodynamic instability play an important role in mix processes: (1) the Rayleigh-Taylor instability, occurring when a fluid pushes another fluid of higher density; (2) the Richtmyer-Meshkov instability, which takes place when a shock wave accelerates a perturbed interface between two fluids of different densities; and (3) the Kelvin-Helmholtz instability, which arises when a nonzero velocity discontinuity exists between the two fluids. The role of hydrodynamic instabilities in initiating turbulent mixing has attracted the interest of leading physicists and mathematicians for many decades and has been the subject of extensive experimental, theoretical and numerical investigations. Most theoretical work has largely been focussed on understanding the macroscopic properties, such as, the size and growth rate of mixing layers. However, a full quantitatve understanding of either macroscopic or microscopic properties (e.g., local concentration and temperature distributions and their effect on chemical reactions) must ultimately rely on numerical simulations. The FronTier simulation is to relate the microscopic properties of the mixing layer to their effects on chemical reactions, such as combustion, that may be taking place in the mixing layer.

In this work, we present some of the ideas and methods that are being used to understand turbulent mixing. These range from relatively simple analytic models to large scale numerical simulations. The emphasis is on verification of the results through mesh convergence studies and careful analysis of numerical algorithms as well as on validation through detailed comparison to experimental observations.

THEORY

Bubble growth rate The speed of a single bubble of a light fluid rising in a cylindrical tube has been measured in experiments. For multiple bubbles, bubble merger models predict the penetration rate of fingers of light fluid into the heavy fluid. For RT mixing, it is observed that the bubbles increase in size, through a process of bubble competition and merger [1, 2, 3, 4]. The new improved three-dimensional (3D) merger model[5] predict not only the growth rate for the bubble (light fluid) interface, but also the bubble height-to-width ratio.

For the case of RT mixing, the bubble penetration height h_b satisfies the scaling law $h_b = \alpha_b A g t^2$, where $A = (\rho_s - \rho_b)/(\rho_s + \rho_b)$ is the Atwood number, t the time, $\rho_{s(b)}$ (s = spike = heavy fluid, b =

bubble = light fluid) the fluid density in the spikes (bubbles), and α_b is called the bubble growth rate that is determined by four directly measurable quantities: (1) The mean merger rate ω; (2) The maximum height separation (h'_m) between two neighbouring bubbles for instantaneous merger. (3) The speed of a single bubble (c_b) in a periodic array. (4) A geometrical factor (k) giving the increase in radius for a single merger event, slightly less than $\frac{1}{2}$. Each of the preceding is expressed in scaled units. The fixed point formula for α_b is given by

$$\alpha_b = \frac{k}{4}\left(c_b + \frac{1+k}{2}h'_m\omega\right)\omega. \qquad (1)$$

For uniform-sized bubbles, $k = 0.414$, $\omega \sim 0.43$, $h'_m \sim 1.82$, taking $c_b = 0.532$ for hexagonal bubbles, then $\alpha_b \approx 0.048$. For non uniform-sized bubbles, α_b increases depending upon the size distribution. If the nonuniformly distributed bubles have a distribution in radius with a variance of $\sim (0-50)\%$, the scaling constant α_b for bubbles in 3-D RT is in the range $\sim 0.05 - 0.06$, a good agreement with experimental results $\sim 0.06 \pm 0.01$ [6, 7, 8]. The same formulas yield the bubble height-to-width ratio $\sim 2.9 - 3.1$ which agrees with experimental data.

Mixing layer properties Buoyancy drag models are based on a phenomenological equation describing the balance of inertial and drag forces acting on both bubbles and spikes that occur in mixing layers. The basic equation [8, 10, 11] is:

$$(\rho_i + k_i\rho_{i'})\frac{dV_i}{dt} = (\rho_i - \rho_{i'})g(t) - (-1)^i\frac{C_i\rho_{i'}V_i^2}{|h_i|}, \quad (2)$$

where the "added mass" coefficient k_i, and the drag coefficient C_i, are the model parameters, $i = 1 = b$ and $i = 2 = s$, $V_i \equiv dh_i/dt$ is the velocity of the edge i of the mixing zone. For given α_b, the growth rate of spikes (α_s) can be obtained by assuming a stationary center of mass of the mixing layer. The results are in good agreement with the Linear Electric Motors (LEM) experiment data [9].

Remarkably, it is possible to solve Equation (2) analytically, thus obtaining explicit expression for the edges of the mixing layer as function of time [12]. To leading orders in t, the result is

$$|h_i(t)| \approx \frac{1}{4a_i^2}Ag(t-t_0)^2 + \frac{\gamma_1}{a_i}(1+f_{i0})^{-1/2a_i^2}\sqrt{Ag|h_{i0}|}(t-t_0) + \frac{\gamma_1^2|h_{i0}|}{(1+f_{i0})^{1/a_i^2}}, \quad (3)$$

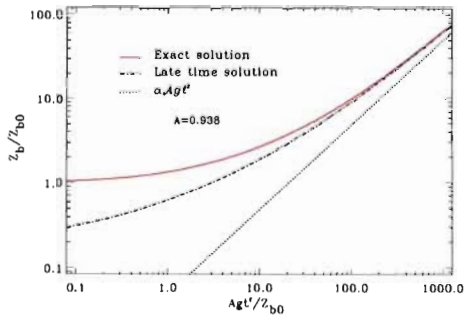

FIGURE 1. The entire dynamical evolution of the trajectory of the RT mixing bubble front for $A = 0.938$ (here $h_b = Z_b$). The solid line represents the exact solution, the dashed line denotes the late time asymptotic solution, and the dotted line gives the pure leading order asymptotic solution.

where $a_i^2 \equiv \frac{1}{2}1 + C_i[1-(-1)^i A]$, $f_{i0} \equiv (1 - a_i|V'_{i0}|)/(1 + a_i|V'_{i0}|)$, $V'_i \equiv V_i/\sqrt{Ag|h_i|}$, and $\gamma_1 \equiv (1+f_{i0})^{\frac{1}{2a_i^2}}(1 + \frac{2f_{i0}}{(1+f_{i0})(1-4a_i^2)})$, $h_{i0} = h_i(t = t_0)$ is the initial position of edge i of the mixing zone. Eq. (3), for the first time, displays the entire dynamical evolution of the trajectory of the RT mixing edges (for both early and late time) in terms of the physical parameters (A, C_i, k_i) and the initial conditions (Fig. 1). It also reveals the dynamical transition of the system from an early (but still chaotically mixing) behavior to the late time self-similarity regime. This solution thus provides a deeper understanding for the self-similarity assumed in the other models. It also shows that the corrections to the leading order expressions ($\sim Agt^2$) for $|h_i|$ depend on the initial conditions, and our expression gives A-dependent drag coefficients if the RT bubble mixing rate α_b is independent of the Atwood number A. These results are consistent with both experiments and numerical simulations.

Solution (3) shows that the RT mixing layer grows exponentially at early times, then linearly during the intermediate stage with a dependence on initial-conditions, and later reaches the self-similarity regime and grows as αAgt^2. The usual αAgt^2 solution is only a late time self-similar solution.

Applying the drag coefficients specified from the RT mixing growth rate to RM mixing ($g = \delta(t)$)

gives an expression for the edges of the RM mixing layer at any time t,

$$|h_i(t)| = |h_{i0}|\left[1 + \frac{(1+2a_i^2)}{2|h_{i0}|}|V_{i0}|(t-t_0)\right]^{\frac{2}{1+2a_i^2}}. \quad (4)$$

This solution shows that the exponents and coefficients in (4) are explicitly related to the drag coefficient, Atwood number and initial conditions. For large t, the trajectory of the mixing front of fluid i has the asymptotic behavior

$$|h_i(t)| \sim |h_{i0}|^{1-(\theta_i)}|V_{i0}|^{\theta_i}\theta_i^{-\theta_i}(t-t_0)^{\theta_i}\ , \quad (5)$$

where $\theta_i \equiv 2/(1+2a_i^2) = 1/\{1 + \frac{C_i|1-(-1)^iA|}{1+(-1)^iA+k_i|1-(-1)^iA|}\}$ $(i = 1,2)$ are scaling model parameters for RM mixing similar to the growth rate α_i in RT mixing. These parameters can be measured in experiments. For $A = 1$, $\theta_s = 1$. These results appear to agree with existing LEM and other experimental data. We also see that unlike RT mixing, the dynamical evolution of the mixing layer in RM mixing always strongly depends on the initial conditions. These solutions provide the clearest explanation offered to date of the often noted fact that RT mixing often (in the absence of long wavelength) loses memory of its initial conditions, while RM mixing does not.

NUMERICAL SIMULATIONS

It is well known that (Eulerian) finite-difference solutions of fluid equations with density discontinuities lead to substantial amounts of numerical mass diffusion. Three facts make mass diffusion particularly important in turbulent mixing simulations. First, the instability itself is driven by density differences, and so mass diffusion acts to mask the driving force of the instability. Second, the interface between the two fluids is unstable, and its area increases very significantly throughout the simulation, thus allowing for enhanced numerical (or physical) mass diffusion in a 3D mixing context. Third, the solutions are computationally expensive, and represent a balance between conflicting objectives, leading to gross under resolution, and consequent substantial numerical mass diffusion. The two conflicting objectives are (1) statistical inclusion of a suffcient number of modes to allow the randomization of mode-mode interactions to have a chance to develop and (2) sufficient numerical resolution per mode to allow accurate simulations. In a typical 3D simulation, the bubbles grow in the z direction and are arranged in a planar array, with some 50×50 modes present initially in the x, y plane, each resolved with about 5×5 mesh cells. The numerical diffusion of a density jump will quickly spread to a width of 3 cells. Under such conditions, much of the density contrast is obliterated by the numerical integration of the equations. The numerical mass diffusion reduced the density contrast by 50%, just about the amount by which the simulation underpredicted experimental results.

Over the years people have developed high-resolution numerical methods specifically designed to avoid numerical mass diffusion. The Front Tracking method developed by the Front Tracking group at Stony Brook and LANL, uses two grid systems. One is a regular grid, and stores the normal fluid variables throughout space. The other is a surface grid, defined on a moving surface (the "front"), which follows (tracks) the moving discontinuity.

Conventionally, difference operators are defined using stencils that may cross the tracked interface. When this occurs these difference stencils and operators are replaced. The state values on the remote side of the interface are replaced with extrapolated ghost-cell state values. In this way the state values associated with the stencil are all taken from a single side of the tracked interface. This ghost-cell algorithm was introduced by Glimm et al in 1980 [13], and has become widely used in other interface algorithms. This method has been improved, through extensions to 3D and robust treatment of topology bifurcations. In a feature which is still experimental, the differencing of the front is completely conservative, and replaces the ghost-cell algorithm. This algorithm has been tested extensively on purely mathematical surface deformation problems of interest to the computational interface community. It has been found to be the best of the methods compared. In comparisons, it has outperformed other methods (including level-set and volume-of-fluids methods).

As one continues to improve the strictly numerical aspects of the front-tracking algorithm, it has been realized that improving the physical modeling and solving equations that better represent physical reality are critical. Normally the simulations are conducted with idealized physics, omitting surface tension (for immiscible fluids), physical mass diffusion

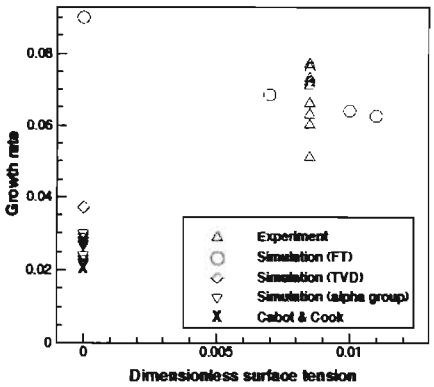

FIGURE 2. The RT growth rate α_b vs. dimensionless surface tension σ. Shown are all experimental values not using surfactants, several front tracking simulations, with varying levels of surface tension including one without use of surface tension, and several untracked simulations without use of surface tension. We note (a) the excellent agreement of the tracked simulations with experiment, (b) the significant dependence of the tracked simulations on surface tension and (c) the discrepancy between the untracked simulations with experiment, with tracked simulations and with each other. (Courtesy of the Front Tracking group at Stony Brook and LANL.)

(for miscible fluids), viscosity and compressibility. The tracked simulation results presented here include all four: surface tension, mass diffusion, viscosity and compressibility. The first three have provided the leading order correction for idealized physics for most of the various experiments previously conducted. As the numerics is of necessity not fully resolved, an important improvement to the simulation was to include subgrid scale (turbulence) models for viscosity and diffusion. The result was a striking success: the simulations, now having both better physics and better numerics, finally agree with experiments (Fig. 2). It is worthwhile to point out that the agreement with experiment also required improved modeling of initial conditions, such as the discussed long-wave-length perturbations ("noise") in some experiments and the width of the initial mass diffusion layer.

Comparison of tracked to untracked simulations clearly indicate that numerical mass diffusion in untracked simulations is a major contributor to the discrepancy. Numerical surface smoothing in the untracked simulations also plays a role in the discrepancy. Figure 3 demonstrates the tracked 3D RT simulations performed by the Front Tracking group at Stony Brook and LANL, in these calculations, the numerical mass diffusion is very low.

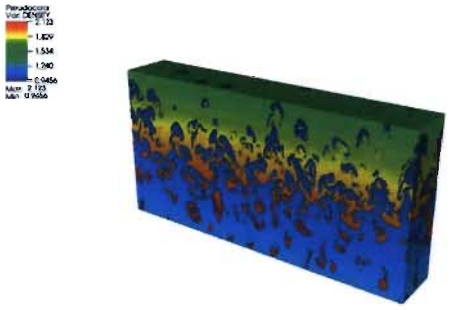

FIGURE 3. The density plot for the tracked 3D Rayleigh-Taylor simulation with experiment #112 of Smeeton-Youngs.

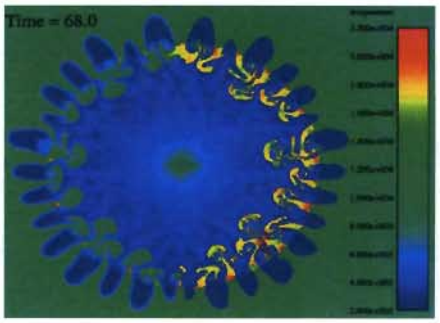

FIGURE 4. The temperature difference between the RAGE and FronTier simulations. The left side is from untracked RAGE simulations and the right side is from tracked FronTier simulations. (Courtesey of the Front Tracking group at Stony Brook and LANL.)

Finally, for further comparison, we demonstrate the simulations for circular RM instabilities at late time, respectively, by Front Tracking (FronTier) and by untracked RAGE (Radiation Adaptive Grid Eulerian) [14], in Fig. 4. The results indicate that the mix structure in FronTier is more complex than in RAGE. For example, the FronTier interface breaks up into droplets whereas the interface in RAGE is smoothed by numerical mass diffusion. At reshock the fingers are heated to a much higher temperature in the FronTier simulation than the corresponding fingers in the

RAGE simulation. The main cause for this is the thermal and mass diffusion at the interface in RAGE and the mixed cell hypothesis at a cell level in RAGE and most other computational fluid dynamics codes. With front tracking, after shock FronTier continues to have a significantly higher maximum temperature.

CONCLUSION

In this paper, we have presented the theoretical predictions for the Rayleigh-Taylor instability growth rate from the bubble merger model and the dynamical evolution of the mixing fronts (bubbles and spikes) for both the Rayleigh-Taylor and Richtmyer-Meshkov instabilities from buoyancy drag model. All theoretical predictions have excellent agreement with experimental data. We have also demonstrated numerical simulations of the 3-D Rayleigh-Taylor problem and the 2-D circular Richtmyer-Meshkov problem with the Front Tracking code in which the numerical mass diffusion is very low. The simulation results from FronTier with an improved front tracking algorithm and improved physics modeling (including surface tension, physical mass diffusion, viscosity and compressibility) on the overall RT growth rate are in good agreement with the experimental data while simulations of others only give a growth rate half or less of the experimental value. Comparison of tracked to untracked simulations from RAGE indicates that numerical mass diffusion in untracked simulations is the primary cause for the discrepancy between simulations and experimental data. Clearly, the tracked simulation has outperformed other methods.

ACKNOWLEDGMENTS

This work was performed under the auspices of the U.S. Department of Energy by the Los Alamos National Laboratory under contract number W-7405-ENG-36.

REFERENCES

1. Sharp, D. H. and Wheeler, J.A., *Late stage of Rayleigh-Taylor instability,* Technical report, Institute of Defense Analyses, 1961.
2. Glimm, J. and sharp, D. H., *Phys. Rev. Lett.*, **64**, pp 2137-2139 (1990).
3. Glimm, J. and Sharp, D. H., *Quarterly J. Appl. Math.*, **56**, pp 741-765 (1998).
4. Oron, D, et al. *Phys. of Plasmas,* **8**, pp 2883-2889 (2001).
5. Cheng, B., Glimm, J. and Sharp, D.H, *Chaos*, **12**, pp 267-274 (2002).
6. Read, R. I., *Physica D*, **12**, pp 45-58 (1984).
7. Smeeton, V. S. and Youngs, D. L., *Experimental investigation of turbulent mixing by Rayleigh-Taylor instability (part 3),* AWE Report Number O 35/87, 1987.
8. Dimonte, G and Schneider, M. *Phys. Fluids*, **12**, pp 304-321 (2000).
9. Dimonte, G and Schneider, M. *Phys. Rev. E*, **54**, pp 3740-3743 (1996).
10. Oron, D, et al. *Laser and Particle Beams*, **17**, pp 465-475 (1999).
11. Cheng, B., Glimm, J. and Sharp, D. H., *Phys. Lett. A*, **268**, pp 366-374 (2000).
12. Cheng, B., Glimm, J. and Sharp, D.H., *Phys. Rev. E*, **66**, pp 036312 (2002).
13. Glimm, J., Marchesin, D. and McBryan, O., *J. Comput. Phys.*, **39**, pp 179-200 (1981).
14. Masser, T. O., *Breaking Temperature Equilibrium in Mixed Cell Hydrodynamics,* Ph.D. thesis, State University of New York at Stony Brook, 2007.
15. Lim, H., et al, *Physica Scripta,* **T142**, pp 1-13 (2009).
16. Lim, H., et al, *J. High Energy density physics,* **6**, pp 223-226 (2009).